


Article

Comparative Study of Thermodynamic Regulation Characteristics in a Dual-Tube Reactor with an External Heat Exchanger

Yong Bai¹, Yunfeng Ma^{1,2,*}, Changjun Ke^{1,2}, Wang Cheng¹, Guangyan Guo¹, Peng Zhao¹, Can Cao¹, Lifan Liao^{1,2}, Xuebo Yang¹  and Zhongwei Fan^{1,2}

¹ Aerospace Information Research Institute, Chinese Academy of Sciences, No. 9 Deng Zhuang South Road, Beijing 100094, China

² School of Optoelectronics, University of Chinese Academy of Sciences, Yuquan Road No. 19, Beijing 100049, China

* Correspondence: mayf100612@aircas.ac.cn

Abstract: A special dual-tube reactor-dual fluidized bed reactor (DFBR), including an external heat exchanger (EHE) and a bypass, was designed to solve the problems that the waste heat of the hot fluid cannot be fully utilized and the reaction temperature cannot be accurately adjusted. Two connection schemes of DFBR and EHE with their thermodynamic equilibrium models and algorithms were proposed, and the optimal scheme was obtained by comparing the outlet temperature and thermal load. The results of the thermodynamic and operating characteristics of the optimal scheme showed that the hot fluid and the cold fluid had positive and negative effects on the heat transfer process, respectively. Increasing the cold fluid mass flow rate in the main stream can enhance the thermal load of the system and increasing the cold fluid mass flow rate in the bypass helped to increase the thermal load of DFBR, even exceeding that of EHE. Adding a bypass can adjust temperature precisely and increasing the inlet temperature can more effectively increase the adjustment range of the reaction zone temperature. The experimental results showed that introducing a bypass can significantly reduce the calculation deviation (12.8%), which decreased with the increasing temperature.

Keywords: bypass; dual fluidized bed reactor; external heat exchanger; numerical simulation; thermodynamic characteristics



Citation: Bai, Y.; Ma, Y.; Ke, C.; Cheng, W.; Guo, G.; Zhao, P.; Cao, C.; Liao, L.; Yang, X.; Fan, Z. Comparative Study of Thermodynamic Regulation Characteristics in a Dual-Tube Reactor with an External Heat Exchanger. *Energies* **2022**, *15*, 6794. <https://doi.org/10.3390/en15186794>

Academic Editors: Nazrul Islam, Dibakar Rakshit, Saleem Anwar Khan, Abdullatif A. Gari, Abdus Samad and Amjad Ali Pasha

Received: 10 August 2022

Accepted: 15 September 2022

Published: 16 September 2022

Publisher's Note: MDPI stays neutral with regard to jurisdictional claims in published maps and institutional affiliations.



Copyright: © 2022 by the authors. Licensee MDPI, Basel, Switzerland. This article is an open access article distributed under the terms and conditions of the Creative Commons Attribution (CC BY) license (<https://creativecommons.org/licenses/by/4.0/>).

1. Introduction

Tubular reactor was the continuous operation reactor with a tubular shape, a large length-to-diameter ratio, no mechanical or movable parts, low back-mixing phenomena, and only relying on different structures of fluid pipelines [1–3], so its volumetric efficiency (production ability of unit volume) was high, which was especially suitable for thermochemical reaction occasions requiring high conversion rate or series reactions and widely used in many fields such as chemical industry, medicine, food, petroleum, environmental protection [4,5]. Among them, the dual-tube reactor was the common one, and its heating zone (outer annular zone) was usually used to provide thermal energy for the reaction zone (inner circular zone) [6–8]. However, since the high-temperature hot fluid in the heating zone still had a higher temperature after heating the cold fluid in the reaction zone and being discharged from the heating zone, its direct discharge can result in a waste of thermal energy [9]. Therefore, it was very important for the design and development of the dual-tube reactor to make full and reasonable use of the waste heat and reduce the input of external thermal energy [10,11].

Generally speaking, the cold fluid entering the reaction zone of the inner tube needs to be preheated in advance to reduce the internal heating time and improve the reaction efficiency. It was a necessary and reasonable way to preheat the cold fluid entering the

reaction zone by the high-temperature hot fluid flowing out of the heating zone. Moreover, to the best of the authors' knowledge, currently, a relatively common application to achieve the above requirements was to equip the dual-tube reactor with an external heat exchanger (EHE) [12]. Many researchers used EHE to control the thermal energy recovery and temperature control of the tubular reactor. To improve the heat transfer efficiency of the dual-tube reactor, some researchers developed a specific heat exchanger. Wang et al. designed a heat exchanger system for a circulating fluidized bed and gasifier, which used the gas flowing out of the EHE to control the flow of hot sand instead of a traditional mechanical method to avoid friction loss and accurately controlled the reaction temperature [13]. Tian et al. designed a system that can simultaneously control the solid flow of two heat exchangers to adjust the heat transfer surface [14].

In addition, the thermal load and temperature control of EHE were also the focus of the design of the dual-tube reactor system, especially for temperature-sensitive thermochemical processes, such as the combustion and pyrolysis of pulverized coal, whose reaction temperature in the reaction zone generally needed to be maintained constant. Therefore, when EHE was applied, its outlet temperature needed to be strictly controlled. Currently, adding a bypass to the heat exchanger was an effective way to control the outlet temperature. Compared with conventional heat exchanger networks, this way can significantly improve adjustment characteristics [15]. The research results of Luyben et al. showed that increasing the effective heat transfer area and the proportion of the bypass flow rate can significantly expand the adjustment range of the overall heat transfer coefficient [16]. Some researchers developed a calculation method for the heat exchanger and its bypass flow rate and valve opening to precisely control the temperature [10,14,17]. Furthermore, many researchers developed mathematical models to determine the optimal parameters of EHE and bypass pipelines [1,4,9,18].

In summary, although there were many studies on the application of EHE to dual-tube reactors, the specific connection schemes of the two were not compared too much. Different connection schemes led to different distributions of the temperature adjustment range and thermal load in the dual-tube reactor [19]. When introducing the bypass adjustment, the temperature adjustment and thermodynamic characteristics of different connection schemes were still unknown, including the influence mechanism of operating parameters on temperature, overall heat transfer coefficient and thermal load, and the changing characteristics of the cold fluid in the main stream with the bypass.

Therefore, we attempted innovatively to introduce EHE and bypass regulation simultaneously for thermodynamic characteristics regulation of dual-tube reactors. The purpose of this article was to utilize a special dual-tube reactor-dual fluidized bed reactor (DFBR), whose inner tube and outer tube were both fluidized beds of excellent heat transfer efficiency, to determine the optimal connection scheme of DFBR and EHE, and make full use of thermal energy. First, two connection methods were proposed with their thermodynamic equilibrium models establishment, a solution algorithm was developed, and the optimal connection scheme was determined by numerical simulation. Then, the thermodynamic and operating characteristics of the optimal connection scheme were obtained by numerical simulation, with emphasis on the temperature and thermal load adjustment characteristics. Finally, the DFBR and EHE experimental apparatus were built to verify the rationality of the selected connection scheme by experiments. The results of this research can provide a novel thermal energy utilization method and an EHE connection method for the tubular reactor, which was of great significance to the development, utilization, and expansion of the tubular reactor.

2. Heating Scheme

To facilitate the recycling of thermal energy, so that the DFBR system can work at low energy-consumption operations, introducing a furnace to generate high-temperature hot fluid (combustion gas) was an ideal heating method [20]. At the same time, adding an EHE (spiral plate heat exchanger) can achieve the heat exchange process between hot

fluid and cold fluid (air at room temperature, as a fluidized carrier gas for the reaction zone). As shown in Figure 1, two common connection schemes of the DFBR and EHE were selected and designed for comparative study, whose difference lay in the flow sequence of the combustion gas (hot fluid in Figure 1). It passed through the DFBR first and then entered the EHE in scheme 1, while it was the opposite in scheme 2. In addition, the cold fluid was divided into a branch ($m_{c,by}$) and directly entered the reaction zone, while the main path ($m_{c,in}$) needs to pass through the EHE. The precise temperature adjustment can be realized by configuring the two flow rates above rationally.

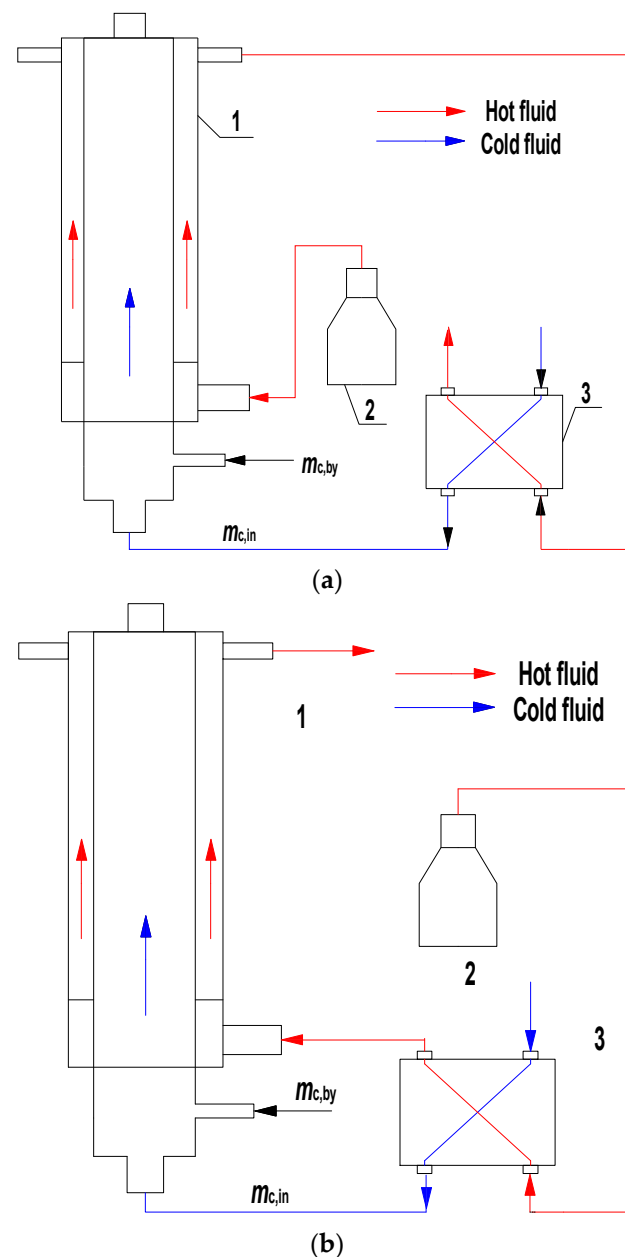


Figure 1. Connection schemes of DFBR and EHE: (1) DFBR; (2) furnace; (3) EHE: (a) scheme 1; (b) scheme 2.

To facilitate the subsequent model establishment and numerical simulation, the main parameters of DFBR and EHE are shown in Tables 1 and 2. In addition, the hot and cold fluids were combustion gas (mainly nitrogen, carbon dioxide, and a small amount of water steam) and air, respectively, whose thermophysical properties at different temperatures can be calculated by interpolation using the data in Tables 3 and 4.

Table 1. Main parameters of DFBR.

Parameter	Value
Inner tube diameter	180 mm o.d., 170 mm i.d.
Outer tube diameter	273 mm o.d., 263 mm i.d.
Inner pipe length	1.4 m
Outer pipe length	1.55 m
Pipes material	310S
Others material	304
Packing type	quartz sand
Quartz sand particles specification	0.256 mm
Quartz sand material	SiO ₂

Table 2. Main parameters of EHE.

Parameter	Value
Board thickness	0.4 m
Board width	0.003 m
Actual heat transfer area	1.7 m ²
Inter-channel spacing	0.02 m
Center circle diameter	0.1 m
Maximum outer diameter	0.658 m
Material	310S

Table 3. Physical properties of combustion gas.

Temperature, °C	Density, (kg/m ³)	Specific Heat Capacity, kJ/(kg·°C)	Conductivity, W/(m·°C)
300	0.755	2.15	0.0556
700	0.566	2.26	0.0683
1000	0.443	2.31	0.0807

Table 4. Physical properties of dry air.

Temperature, °C	Density, (kg/m ³)	Specific Heat Capacity, kJ/(kg·°C)	Conductivity, W/(m·°C)
20	1.205	1.00	0.0259
350	0.566	1.06	0.0419
1000	0.277	1.18	0.0807

3. Development of Thermodynamic Equilibrium Model

A comparative analysis of the two connection schemes was carried out by theoretical calculation methods in this section. Simplify the connection schemes and establish the thermodynamic equilibrium models to describe the mathematical relationship between the operating parameters and the adjustment object. Meanwhile, the operating characteristics of the DFBR can be easily obtained to evaluate the rationality of the DFBR system connection scheme by numerical simulation.

3.1. Model Establishment

It was known that the whole system was composed of DPFB and EXE, and DPFB can also be regarded as a heat exchanger, so the whole system can be regarded as a heat exchanger network in which two heat exchangers were connected in a certain way. For convenience, DPFB was referred to as the main heat exchanger below and the two thermodynamic equilibrium models of the two schemes were shown in Figure 2.

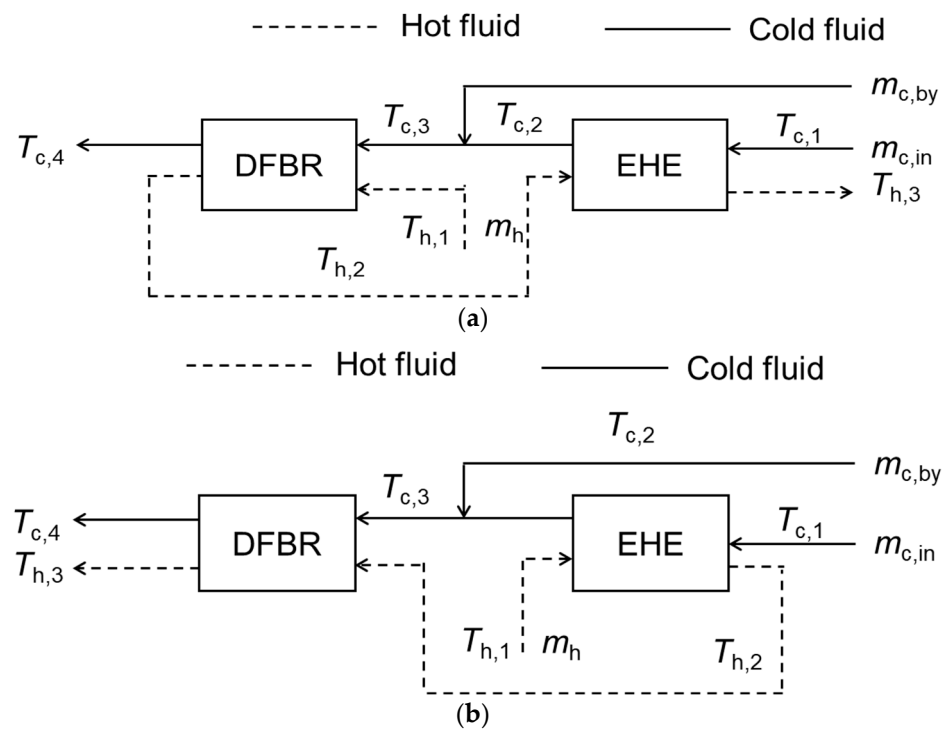


Figure 2. Thermodynamic equilibrium model of DFBR and EHE: (a): scheme 1; (b): scheme 2.

Here, some basic assumptions were as follows:

- (1) Ignore the effect of gravity on the gas;
- (2) The kinetic energy of gas was conserved;
- (3) Gas and solid mass were conserved;
- (4) Ignore the temperature gradient in the radial direction of the inner tube;
- (5) Ignore the effect of temperature on the physical properties of particles and metal containers;
- (6) The particle size distribution was uniform and ignore deformation and cracking;
- (7) Ignore the effect of radiation heat transfer.

According to the thermodynamic equilibrium model, the corresponding mathematical relationship can be established. Here, scheme 1 was taken as an example to summarize the establishment steps of a mathematical relationship. First, based on the conservation of energy and mass, the following equations were obtained [21,22]:

$$Cp_h m_h (T_{h,1} - T_{h,2}) = Cp_c m_c (T_{c,4} - T_{c,3}) \quad (1)$$

$$Cp_h m_h (T_{h,2} - T_{h,3}) = Cp_c m_{c,in} (T_{c,2} - T_{c,1}) \quad (2)$$

$$m_c = m_{c,in} + m_{c,by} \quad (3)$$

$$Cp_c m_{c,in} (T_{c,2} - T_{c,3}) = Cp_c m_{c,by} (T_{c,3} - T_{c,1}) \quad (4)$$

Next, the heat transfer constitutive equations were established and closed. The internal heat transfer process of the main heat exchanger and EHE can be described by the following equations:

$$Q_1 = A_1 K_1 t_{m1} \quad (5)$$

$$Q_2 = A_2 K_2 t_{m2} \quad (6)$$

The effective heat transfer area of the main heat exchanger was a known amount. Furthermore, this EHE was a spiral plate heat exchanger whose heat exchange method was countercurrent heat exchange, whose main structural parameters were shown in Table 3, and whose effective heat transfer area was larger than DFBR (the outer surface area of the inner tube).

The overall heat transfer coefficient K_1 of DFBR can be calculated by our previous research results [23]:

$$K_1 = \frac{1}{\frac{d_2}{\alpha_{gs1}d_1} + \frac{d_2}{\alpha_{gs2}d_1} + \frac{d_2}{\alpha_{sw1}d_1} + \frac{1}{\alpha_{sw2}} + \frac{\delta_1 d_2}{\lambda_1 d_1}} \quad (7)$$

The overall heat transfer coefficient K_2 of EHE can be obtained by the classic heat transfer equations. If the effect of impurities on heat transfer were ignored, there were [21]:

$$K_2 = \frac{1}{\frac{1}{\alpha_h} + \frac{\delta_2}{\lambda_2} + \frac{1}{\alpha_c}} \quad (8)$$

$$\alpha_x = 8.4 \frac{\lambda_x}{d_{e,x2}} \left(\frac{m_x C p_x}{\lambda_x l_x} \right)^{0.2} \quad (9)$$

In summary, considering DFBR and EHE as an adiabatic system and ignoring the thermal energy dissipation of the connecting tubes, the following thermodynamic equilibrium relationships can be obtained:

$$\begin{cases} Q_1 = C p_h m_h (T_{h,1} - T_{h,2}) \\ Q_1 = C p_c m_c (T_{c,4} - T_{c,3}) \\ Q_1 = A_1 K_1 t_{m1} \\ t_{m1} = \frac{t_{11} - t_{12}}{\ln\left(\frac{t_{11}}{t_{12}}\right)} \\ t_{11} = T_{h,1} - T_{c,3} \\ t_{12} = T_{h,2} - T_{c,4} \end{cases} \quad (10)$$

$$\begin{cases} Q_2 = C p_h m_h (T_{h,2} - T_{h,3}) \\ Q_2 = C p_c m_{c,in} (T_{c,2} - T_{c,1}) \\ m_c = m_{c,in} + m_{c,by} \\ C p_c m_{c,in} (T_{c,2} - T_{c,3}) = C p_c m_{c,by} (T_{c,3} - T_{c,1}) \\ Q_2 = A_2 K_2 t_{m2} \\ t_{m2} = \frac{t_{21} - t_{22}}{\ln\left(\frac{t_{21}}{t_{22}}\right)} \\ t_{21} = T_{h,3} - T_{c,1} \\ t_{22} = T_{h,2} - T_{c,2} \end{cases} \quad (11)$$

3.2. Algorithm Development

DFBR and EHE can be meshed along the effective heat exchange surface, then Equations (10) and (11) can be iteratively solved by the one-dimensional finite difference method. For Equation (10), the calculation started and solved from the fluid inlet until the last grid. Due to the relatively short grid length, Equation (10) can be simplified and discrete as follows:

$$\begin{cases} \Delta Q_1^i = C p_h m_h (T_h^i - T_h^{i+1}) \\ \Delta Q_1^i = C p_c m_c (T_c^i - T_c^{i+1}) \\ \Delta Q_1^i = \Delta A_1 K_1^i t_{m1}^i \\ t_{m1}^i = T_h^i - T_c^i \end{cases} \quad (12)$$

Then, the total amount of heat transfer in DFBR was:

$$Q_1 \approx \sum_{i=1}^n \Delta Q_1^i \quad (13)$$

The solution can be achieved when the inlet boundary conditions of DFBR were known. However, since the inlet temperature of cold fluid $T_{c,3}$ of DFBR was unknown, and the EHE was a countercurrent heat exchanger, the above calculation cannot be carried out.

To start the iterative calculation, a hypothetical value at a certain node needed to be given. Start to calculate at the inlet cold fluid of EHE, given an initial value $T_{h,3}[0]$ at the hot fluid outlet, $T_{c,2}$ and $T_{h,2}$, can be solved and derived. Then, $T_{c,2}$ and $T_{h,1}$ can be taken as the starting point to solve to get $T_{c,4}$ and $T_{h,2}$, and $T_{h,3}$ can be obtained. Finally, the difference between $T_{h,3}$ and $T_{h,3}[0]$ was calculated and iteratively checked to obtain an approximate solution. A program was written to realize the calculation, whose program flow was shown in Figure 3.

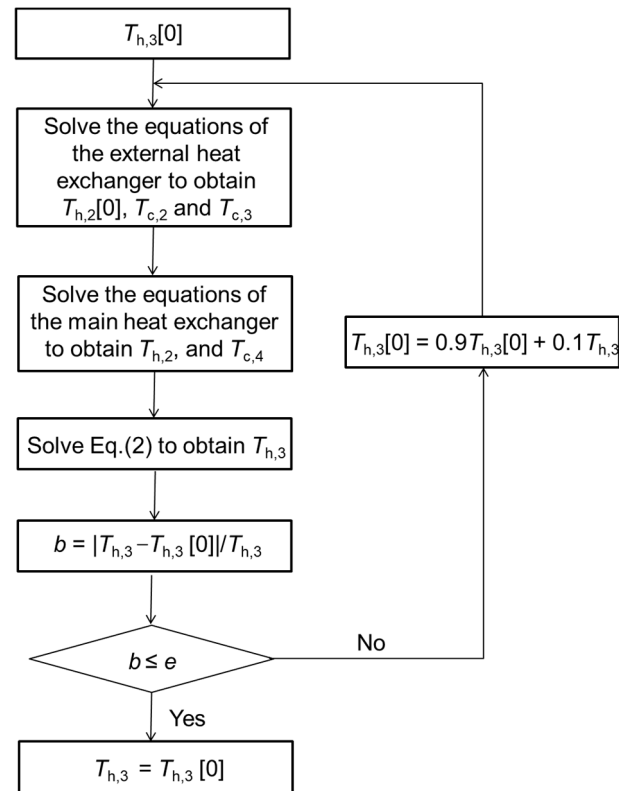


Figure 3. Calculation flow chart of the thermodynamic equilibrium reactor model.

e was the allowed deviation and set to 0.1%.

According to our previous research results, the number of grids was set to 10,000 to minimize the calculation accuracy and minimize the calculation time [24]. The developed model can be used to calculate the temperature and overall heat transfer coefficient of the outlet and other positions of DFBR when the inlet boundary conditions were known. On the contrary, if the temperature and fluid flow rate of a certain position were known, the related inlet parameters can also be deduced.

4. Numerical Simulation

In the same way, the thermodynamic equilibrium model of scheme 2 was also established. Based on the developed model, numerical simulation was carried out to analyze the two schemes comparatively. Subsequently, further studies of the preferred scheme were carried out to analyze the thermodynamic and operating characteristics of DFBR and EHE.

4.1. Comparison of the Two Connection Schemes

First, the mathematical models of the two schemes were solved, respectively, to obtain their basic thermodynamic characteristics for comparative analysis. The mass flow rates of the hot fluid and cold fluid in the main stream were fixed at $m_h = 0.0042$ kg/s and $m_{c,in} = 0.0008$ kg/s, respectively. The changing trend of the outlet temperature and thermal load with the bypass flow rate ($m_{c,by}$) were obtained, as shown in Figure 4. In Figure 4a, it can be seen that for scheme 2, with the increase of $m_{c,by}$, the temperature difference

between the hot and cold fluid gradually increased, but it was not obvious, and the outlet temperature of the hot fluid was always higher than that of the cold fluid. This was because DFBR was a parallel flow heat exchanger, where the direction of the fluid in the heating zone and the reaction zone was the same and the outlets were on the same side. In contrast, the outlet temperature of the hot fluid in scheme 1 was lower than that of the cold fluid, and lower than the outlet temperature of the hot fluid in scheme 2 under the same working conditions, indicating that the thermal energy utilization efficiency of scheme 1 was better. In Figure 4b, the thermal load of the two schemes was compared, and it can be seen that the thermal load of DFBR in scheme 1 was higher while the thermal load of EHE in scheme 2 was higher. In addition, compared with scheme 2, the thermal load in scheme 1 was more sensitive to $m_{c,by}$ and had a larger adjustment range. In summary, scheme 1 was more suitable for DFBR and EHE.

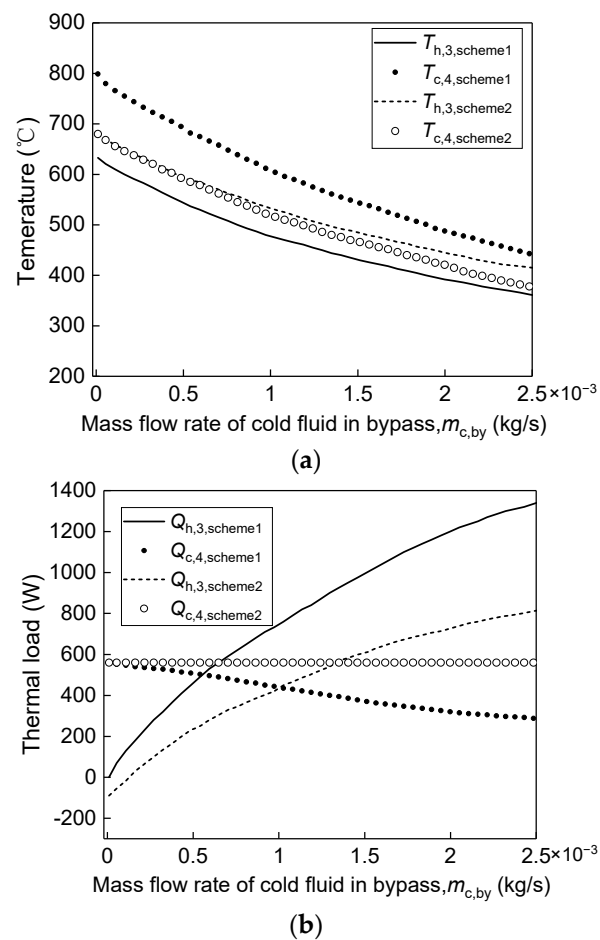


Figure 4. Comparison of thermodynamic characteristics of two connection schemes: (a) outlet temperature; (b) thermal load.

4.2. Thermodynamic Characteristics

When m_h , $m_{c,in}$, and $m_{c,by}$ were taken as independent variables, respectively, to calculate the outlet temperatures under the conditions that $T_{c,1} = 30$ °C and $T_{h,1} = 850$ °C, and the results were shown in Figure 5. In Figure 5a, it can be seen that as m_h increased, $T_{c,4}$ and $T_{h,3}$ both increased, and whether increasing $m_{c,in}$ or $m_{c,by}$ had a negative effect on the outlet temperature, as shown in Figure 5b,c. This was because the hot fluid was the thermal source of the entire system, and increasing m_h can inevitably increase $T_{c,4}$ and $T_{h,3}$, while the cold fluid absorbed thermal energy, and increasing $m_{c,in}$ and $m_{c,by}$ can increase the absorption of thermal energy.

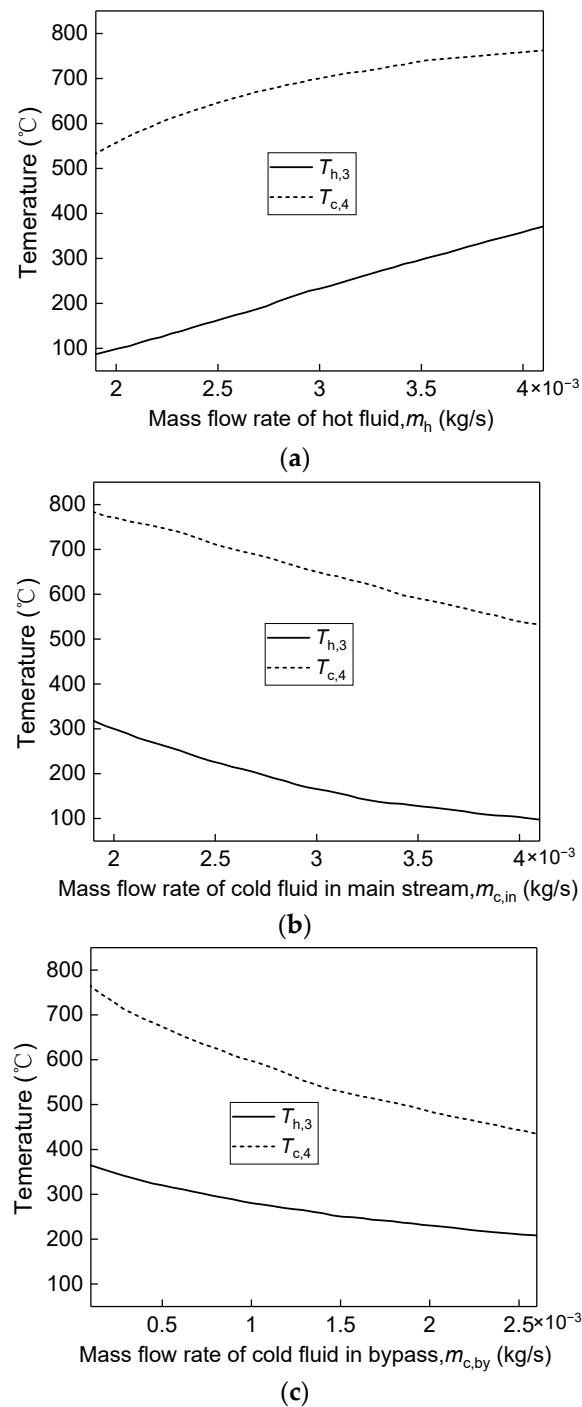
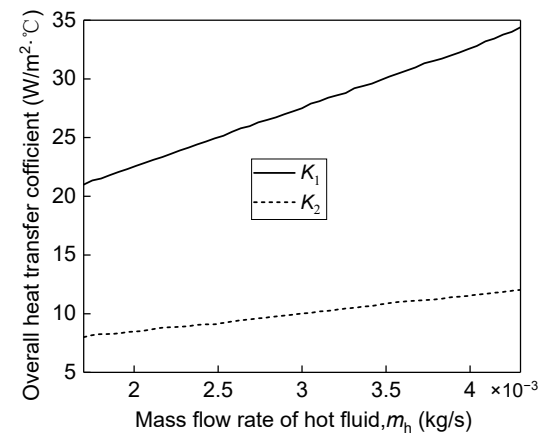


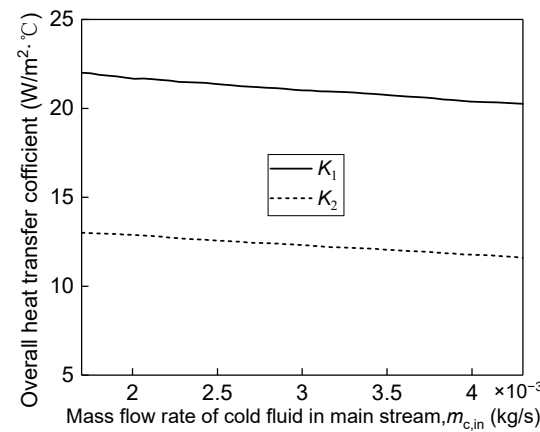
Figure 5. The relationship between the mass flow rate of fluid and the outlet temperatures of reactor: (a) $m_{c,in} = 0.0042$ kg/s, $m_{c,by} = 0$; (b) $m_h = 0.0042$ kg/s, $m_{c,by} = 0$; (c) $m_h = 0.0042$ kg/s, $m_{c,in} = 0.002$ kg/s.

Similarly, the effect of fluid mass flow rate on the overall heat transfer coefficient was studied, as shown in Figure 6. It can be seen that K_1 was higher than K_2 , which was the result of the fluidized bed in DFBR promoting the heat transfer process. m_h had a positive effect on K_1 and K_2 because the fluid mass flow rate was proportional to the gas velocity, whose increase can promote the heat transfer process. It can also be observed that the cold fluid (main stream and bypass) had a certain negative effect on K_1 and K_2 . This was because the increasing $m_{c,in}$ or $m_{c,by}$ decreased the average temperature of the hot and cold fluids, and thus the fluid thermal conductivity also decreased, which was proportional to

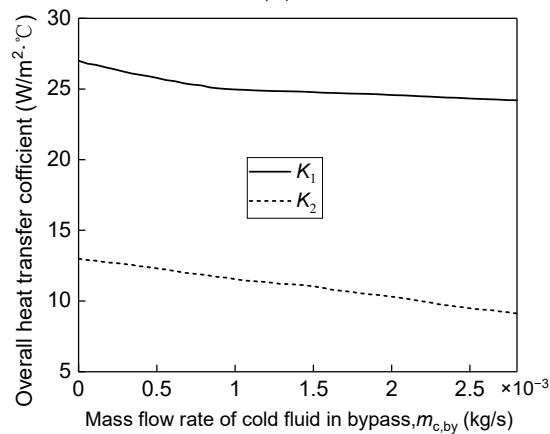
K_1 and K_2 . This phenomenon showed that the effect of fluid thermal conductivity on heat transfer efficiency was also very significant.



(a)



(b)



(c)

Figure 6. The relationship between the mass flow rate of fluid and the overall heat transfer coefficients of DPFBR and EHE: (a) $m_{c,in} = 0.0042$ kg/s, $m_{c,by} = 0$; (b) $m_h = 0.0042$ kg/s, $m_{c,by} = 0$; (c) $m_h = 0.0034$ kg/s, $m_{c,in} = 0.002$ kg/s.

Next, the relationship between the thermal load of DPFBR and EHE with the fluid mass flow rate was calculated. The thermal load referred to the total heat transfer amount, as shown in Figure 7, where Q_t was the sum of Q_1 and Q_2 . It can be seen that the increasing m_h , $m_{c,in}$, and $m_{c,by}$ can increase Q_t . However, as shown in Figure 7a, Q_1 decreased with the increasing m_h , which was mainly because the increase of m_h reduced the average temperature difference between the cold and hot fluids in DPFBR. Meanwhile, as shown in

Figure 7b, as $m_{c,in}$ increased, Q_1 continued to rise, which was the result of the increase in the average temperature difference. While Q_2 first rose and then fell, which was caused by the increase in temperature difference between the hot and cold fluids in EHE cannot keep up with the decrease in the cold fluid thermal conductivity. Although the fluid thermal conductivity in DFBR also decreased, due to the existence of the fluidized bed, the heat transfer efficiency was still higher. It can be seen in Figure 7c that as $m_{c,by}$ increased, the heat transfer of DFBR gradually became dominant. This was because the fluid in the bypass directly entered the reaction zone, which not only promoted the heat transfer efficiency of the fluidized bed in the reaction zone but also expanded the temperature difference between cold and hot fluids. This phenomenon also highlighted the great role played by the fluidized bed in the process of convective heat transfer. However, from the comparison of Figure 7b,c, the same increase in the mass flow rate of the cold fluid, increasing $m_{c,in}$ can achieve a higher Q_t , which confirmed the excellent effect of the combination of DFBR and EHE. Increasing the fluid mass flow rate of the main stream enabled the two heat exchangers to be fully utilized and improved the overall heat transfer efficiency. The temperature of the cold fluid in the bypass was greatly increased after being heated by DFBR, which reduced the average temperature difference of EHE and heat transfer efficiency. The purpose of effectively distributing the thermal load can be achieved by adjusting the mass flow rate ratio of the cold fluid in main stream and bypass, which also reflected the role of the bypass flow.

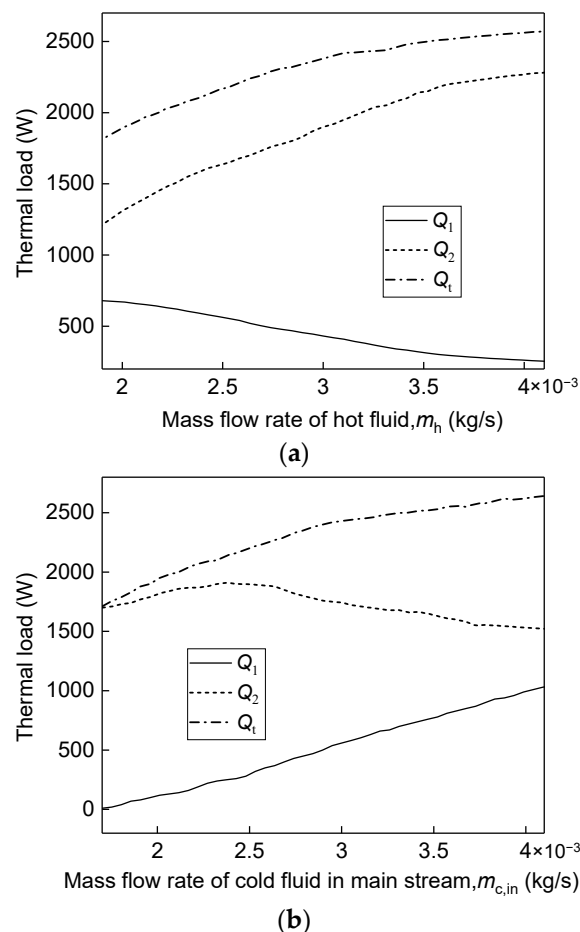


Figure 7. Cont.

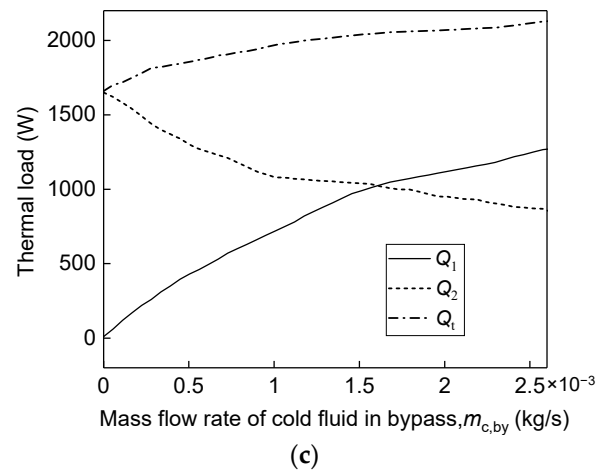


Figure 7. The relationship between the mass flow rate of fluid and the thermal loads of DPF and EHE: (a) $m_{c,in} = 0.0034$ kg/s, $m_{c,by} = 0$; (b) $m_h = 0.0034$ kg/s, $m_{c,by} = 0$; (c) $m_h = 0.0034$ kg/s, $m_{c,in} = 0.002$ kg/s.

4.3. Operating Characteristics

The temperature adjustment characteristics were studied to evaluate the operating characteristics of the entire system. The mass flow rate in the bypass had a significant impact on the heat transfer and thermodynamic characteristics. To further explore the operating characteristics of the DFBR and EHE, $m_{c,by}$ was used as a variable to investigate the changing trend between the internal temperature of the reaction zone and other parameters.

The cold fluid in the bypass was mainly used to adjust the temperature separately. Therefore, when $v_{c,in} = 0.36$ m/s and $v_{h,in} = 0.0042$ m/s were fixed, the relationship between $T_{c,4}$, $m_{c,by}$ and $m_{c,in}$, was obtained, as shown in Figure 8. It can be seen that $m_{c,by}$ decreased with the increasing $m_{c,in}$, but $T_{c,4}$ rose. This was because $m_{c,in}$ was heated by EHE, which helped a lot to increase $T_{c,4}$. However, the sum of $m_{c,in}$ and $m_{c,by}$ was not constant, this was because the physical properties of the fluids changed with the temperature. Nevertheless, $T_{c,4}$, $m_{c,by}$ and $m_{c,in}$ still showed a strong linear relationship, which proved that adjusting $m_{c,in}$ had a certain degree of reliability for $T_{c,4}$. In Figure 8b, when m_h increased, the temperature adjustment range increased because the total thermal energy input was increased. In Figure 8c, $T_{h,1}$ rose from 800 °C to 900 °C, and the adjustment range of $T_{c,4}$ significantly increased. From this point of view, compared with increasing $m_{c,in}$, increasing $T_{h,1}$ can more effectively increase the temperature adjustment range of DFBR inside. In general, the way of adding bypass to EHE can theoretically adjust the temperature in the reaction zone while keeping $v_{c,in}$ constant, and there was a good linear relationship between the outlet temperature of the reaction zone and $m_{c,by}$.

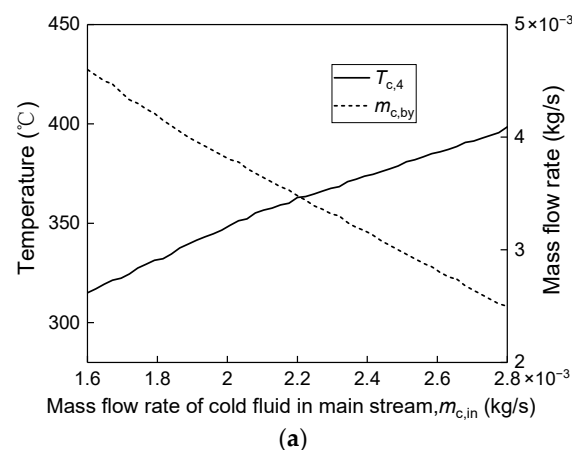


Figure 8. Cont.

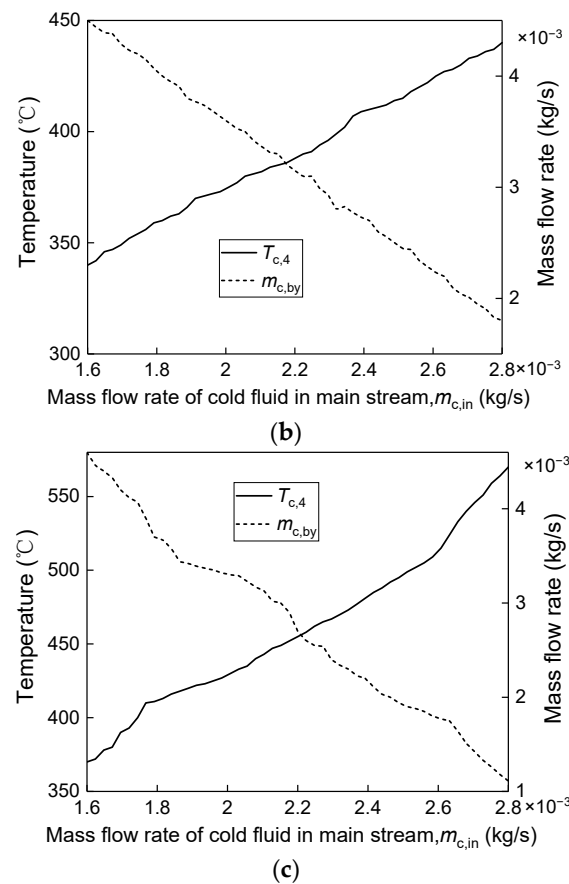


Figure 8. The relationship between the mass flow rate of cold fluid in main stream and the regulation of bypass: (a) $m_h = 0.0042$ kg/s, $T_{h,1} = 850$ °C; (b) $m_h = 0.0045$ kg/s, $T_{h,1} = 850$ °C; (c) $m_h = 0.0042$ kg/s, $T_{h,1} = 1000$ °C.

5. Experimental Verification

5.1. Apparatus and Method

Finally, the experimental verification of the theoretical calculation results of the thermodynamic characteristics was carried out. In this section, the designed DFBR had its own EHE, a spiral plate heat exchanger, whose structural parameters were shown in Table 2. In order to verify the rationality of the connection scheme, a furnace was designed, whose outlet was directly connected to the outer tube of DFBR for combustion. The DFBR and EHE experimental apparatus was shown in Figure 9 [25]. According to scheme 1, the EHE was placed at the bottom of DFBR. The cold fluid outlet can be directly connected to the reaction zone, while the heating zone is connected to the hot fluid inlet through a pipeline. The cold fluid inlet in the bypass was added to the side of the reaction zone. The fuel was liquefied petroleum gas with a calorific value of about 88 MJ/kg. The compressed gas was used to provide air for the furnace and fluidized carrier gas in the reaction zone. Ball valves adjusted the fluid mass flow rate. Thermocouples were installed in the reaction zone, heating zone of DFBR, and each nozzle of EHE to detect temperature. Some thermocouples, pressure meters and flow valves were used as sensors.

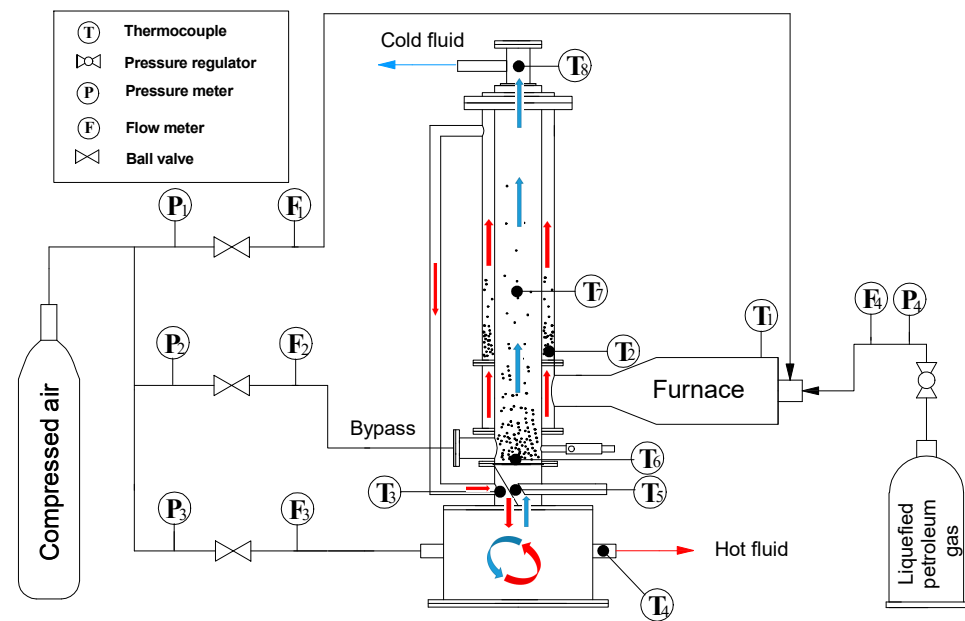


Figure 9. Schematic diagram of the DFBR and EHE experimental apparatus (red arrows: hot fluid; blue arrows: cold fluid).

This content was to measure the temperature of each position of DFBR and EHE under the fixed fluid mass flow rate and compare it with the theoretical calculation results. In order to facilitate operation, maintain the outlet temperature and mass flow rate of the furnace, and change the mass flow rate of the two cold fluids.

5.2. Results and Discussion

The outlet temperature of the reaction zone ($T_{c,4}$ in Figure 2) under different cold fluid mass flow rates was measured and compared with the calculated results. Figure 10a was the relationship of $T_{c,4}$ and $m_{c,in}$ when $m_{c,by}$ was 0. It can be seen that the calculated values were in good agreement with the measured values. As $T_{c,4}$ increased, the deviation also increased towards 12.8%. This was mainly due to the increase in thermal energy loss after $T_{c,4}$ rose. Subsequently, $m_{c,by}$ was increased to 7×10^{-4} kg/s, and the result was shown in Figure 10b. It can be seen that $T_{c,4}$ decreased significantly, because the total absorption of thermal energy of the cold fluid increased at this time, and the calculation deviation also decreased significantly due to the decrease in temperature, which was about 5.4%.

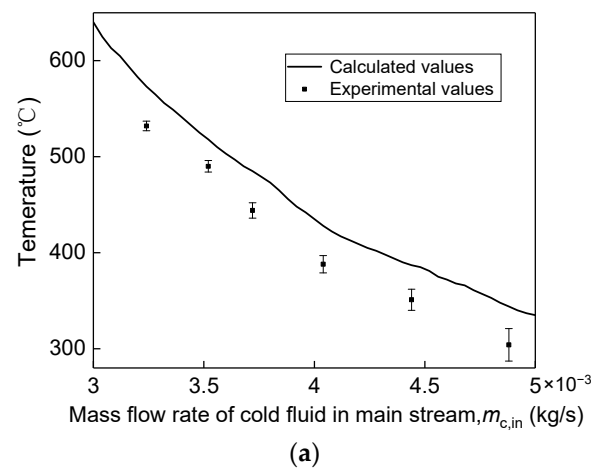


Figure 10. Cont.

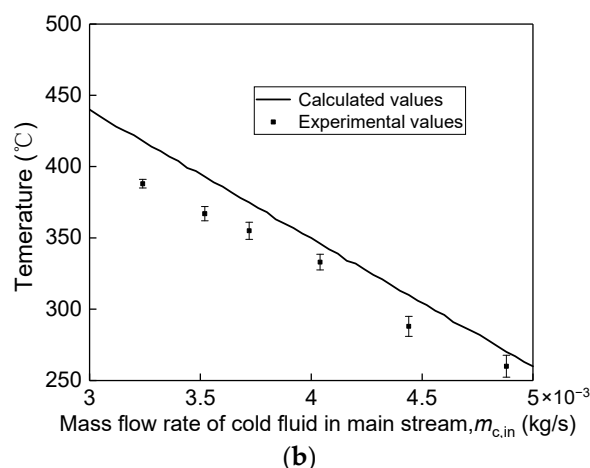


Figure 10. Comparison of the outlet temperatures of reactor between calculated and experimental values of $T_{c,4}$: (a) cold fluid in main stream: $m_h = 0.0042$ kg/s, $T_{h,1} = 850$ °C, $m_{c,by} = 0$; (b) cold fluid in main stream: $m_h = 0.0042$ kg/s, $T_{h,1} = 850$ °C, $m_{c,by} = 7 \times 10^{-4}$ kg/s.

In summary, the theoretical calculation results of thermodynamic characteristics were highly reliable and can be used in the thermodynamic calculations of the DFBR system to investigate the rationality of the scheme. Meanwhile, the test results also confirmed the design of the tubular reactor structure, thermal energy supply, and effect of connection of DFBR and EHE.

6. Conclusions

In this study, two connection schemes of DFBR and EHE, including a bypass, with their thermodynamic equilibrium model were proposed. The heat transfer equations and algorithm were established and the optimal one was selected by numerical simulation. Then, the thermodynamic and operating characteristics were studied to obtain the adjustment range of temperature and fluid mass flow rate. Finally, the DFBR and EHE experimental apparatus were set up to verify the rationality of the scheme. The main conclusions were as follows:

- (1) DFBR was taken as the main body, and the design idea of the tubular reactor system was proposed. EHE was added to improve thermal energy utilization efficiency and a bypass was introduced to achieve precise temperature adjustment, and two connection schemes were proposed.
- (2) A thermodynamic equilibrium model of the reactor system was established and a solution algorithm was proposed. The effects of the two connection schemes were compared by numerical simulation and scheme 1 had higher thermal energy utilization efficiency. In addition, the thermal loads of scheme 1 were more sensitive to the cold fluid flow rate in the bypass, which had a larger adjustment range and was suitable for DFBR and EHE.
- (3) The basic thermodynamic and operating characteristics of the optimal scheme were carried out by numerical simulation further. The existence of the fluidized bed promoted convective heat transfer with a higher overall heat transfer coefficient of DFBR. Compared with increasing the fluid mass flow rate, increasing the inlet temperature can more effectively increase the adjustment range of temperature in the reaction zone inside.
- (4) The experimental verification was carried out and the results showed that the calculated values obtained by the developed model were in good agreement with the experimental values, and the calculation deviation decreased with the decrease in temperature.

Author Contributions: Conceptualization, Y.B. and Y.M.; methodology, Y.B.; software, Y.B.; validation, Y.B., C.K. and W.C.; formal analysis, Y.B. and G.G.; investigation, Y.B. and P.Z.; resources, Y.B. and C.C.; data curation, Y.B. and L.L.; writing—original draft preparation, Y.B. and X.Y.; writing—review and editing, Y.B. and Y.M.; visualization, Y.B. and Z.F.; supervision, Y.B. and Y.M.; project administration, Y.B.; funding acquisition, Y.M. All authors have read and agreed to the published version of the manuscript.

Funding: This research was supported by the fund of the Youth Innovation Promotion Association, CAS, No. Y2021048, Research Group of Short Pulse Laser Technology of Chinese Academy of Sciences, Condition Guarantee and Finance Department (No. GJJSTD20200009).

Institutional Review Board Statement: Not applicable.

Informed Consent Statement: Not applicable.

Data Availability Statement: The study did not report any data.

Acknowledgments: All workers are acknowledged. The writers also acknowledge the assistance of the anonymous reviewers.

Conflicts of Interest: The authors declare no conflict of interest.

Nomenclature

Acronyms

DTBR dual fluidized bed reactor
EHE external heat exchanger

Symbols

A_1 effective surface area of heat transfer in DFBR, m^2
 A_2 effective surface area of heat transfer in EHE, m^2
 Cp_c specific heat capacity, $J/(kg \cdot ^\circ C)$
 d_1 diameter of the inner tube in DFBR, mm
 d_2 radius of the outer tube in DFBR, mm
 d_e hydraulic diameter of tube section, m
 i grid unit number, —
 K_1 overall heat transfer coefficient in DFBR, $W/(m^2 \cdot ^\circ C)$
 K_2 overall heat transfer coefficient in EHE, $W/(m^2 \cdot ^\circ C)$
 l tube length, m
 m_h mass flow rate of the hot fluid, kg/s
 $m_{c,in}$ mass flow rate of the cold fluid in the main stream, kg/s
 $m_{c,by}$ mass flow rate of the cold fluid in the bypass, kg/s
 n total number of grids, —
 Q_1 amount of the thermal energy in DFBR, W
 Q_2 amount of the thermal energy in EHE, W
 Q_t amount of the thermal energy in the whole system, W
 T temperature, $^\circ C$
 t_{m1} logarithmic mean temperature in DFBR, $^\circ C$
 t_{m2} logarithmic mean temperature in EHE, $^\circ C$
 t_{m1}^i logarithmic mean temperature of the i -th grid in DFBR, $^\circ C$
 $v_{c,h}$ velocity of the hot fluid, m/s
 $v_{c,in}$ velocity of the cold fluid in the main stream, m/s
 $v_{c,by}$ velocity of the cold fluid in the bypass, m/s
 ΔA_1 effective heat transfer area of a single grid, W
 ΔQ_1^i amount of the thermal energy of the i -th grid in DFBR, W

Greek Letters

α heat transfer coefficient in EHE, $W/(m^2 \cdot ^\circ C)$
 α_{gs1} heat transfer coefficient between fluid and solid in the inner tube of DFBR, $W/(m^2 \cdot ^\circ C)$
 α_{gs2} heat transfer coefficient between fluid and solid in the outer tube of DFBR, $W/(m^2 \cdot ^\circ C)$

α_{sw1}	heat transfer coefficient between the vessel and solid in the inner tube of DFBR, $W/(m^2 \cdot ^\circ C)$
α_{sw2}	heat transfer coefficient between the vessel and solid in the outer tube of DFBR, $W/(m^2 \cdot ^\circ C)$
δ_1	thickness of inner tube in DFBR, m
δ_2	thickness of spiral plate wall, m
λ_1	thermal conductivity of DFBR, $W \cdot (m \cdot ^\circ C)$
λ_2	thermal conductivity of EHE, $W \cdot (m \cdot ^\circ C)$
Subscripts	
c	cold fluid
h	hot fluid
x	cold fluid or hot fluid
out	gas outlet parameters
s	solid
w	the vessel wall

References

- Otarod, M.; Supkowski, R.M. Low Reynolds number isotope transient kinetic modeling in isothermal differential tubular catalytic reactors. *AIChE J.* **2018**, *64*, 1317–1329. [[CrossRef](#)]
- Major-Godlewska, M.; Radecki, D. Experimental analysis of gas hold-up for gas-liquid system agitated in a vessel equipped with two impellers and vertical tubular baffles. *Pol. J. Chem. Technol.* **2018**, *20*, 7–12. [[CrossRef](#)]
- Alipour-Dehkordi, A.; Khademi, M.H. Use of a micro-porous membrane multi-tubular fixed-bed reactor for tri-reforming of methane to syngas: CO₂, H₂O or O₂ side-feeding. *Int. J. Hydrogen Energy* **2019**, *44*, 32066–32079. [[CrossRef](#)]
- Petunin, A.B.; Sharapaev, A.I.; Muradova, A.G. Tubular Metal Membranes for Cleaning the Primary-Circuit Coolant of a Pressurized Water Reactor (WWER). *Petrol. Chem.* **2017**, *57*, 536–541. [[CrossRef](#)]
- Wang, X.G.; Tian, B.H.; Wang, C.H.; Wu, J.H. Mathematical modelling of residence time distribution in tubular loop reactors. *Can. J. Chem. Eng.* **2017**, *95*, 1101–1108. [[CrossRef](#)]
- Yang, W.J.; Hong, M.H.; Choi, K.Y. Mathematical modeling and analysis of an interfacial polycarbonate polymerization in a continuous multizone tubular reactor. *Polym. Eng. Sci.* **2018**, *58*, 438–446. [[CrossRef](#)]
- Li, Y.H.; Hong, J.R. Performance assessment of catalytic combustion-driven thermophotovoltaic platinum tubular reactor. *Appl. Energy* **2018**, *211*, 843–853. [[CrossRef](#)]
- Beniich, N.; El Bouhtouri, A.; Dochain, D. Constrained global adaptive controller for a plug-flow tubular reactor with partial temperature measurements. *Ima. J. Math. Control Inf.* **2019**, *36*, 1089–1104. [[CrossRef](#)]
- Liu, K.F.; Zhao, J.; Zhu, D.; Meng, F.; Kong, F.H.; Tang, Y.C. Oxidative coupling of methane in solid oxide fuel cell tubular membrane reactor with high ethylene yield. *Catal. Commun.* **2017**, *96*, 23–27. [[CrossRef](#)]
- Mottaghi, M.; Kuhn, S. Numerical investigation of well-structured porous media in a milli-scale tubular reactor. *Chem. Eng. Sci.* **2019**, *208*, 115146. [[CrossRef](#)]
- Diaz, J.P.; Inostroza, C.; Fernandez, F.G.A. Fibonacci-type tubular photobioreactor for the production of microalgae. *Process Biochem.* **2019**, *86*, 1–8. [[CrossRef](#)]
- Xu, J.W.; Li, J.; Ding, Y.D.; Fu, Q.; Cheng, M.; Liao, Q. Numerical simulation of the flow and heat-transfer characteristics of an aligned external three-dimensional rectangular-finned tube bank. *Appl. Therm. Eng.* **2018**, *145*, 110–122. [[CrossRef](#)]
- Wang, Q.H.; Luo, Z.Y.; Fang, M.X.; Ni, M.J.; Cen, K.F. Development of a new external heat exchanger for a circulating fluidized bed boiler. *Chem. Eng. Process. Process Intensif.* **2003**, *42*, 317–335. [[CrossRef](#)]
- Tian, Z.; Gu, B. Analyses of an integrated thermal management system for electric vehicles. *Int. J. Energy Res.* **2019**, *43*, 5788–5802. [[CrossRef](#)]
- Zhuang, Y.; Liu, L.L.; Zhang, L.; Du, J. Upgraded Graphical Method for the Synthesis of Direct Work Exchanger Networks. *Ind. Eng. Chem. Res.* **2017**, *56*, 14304–14315. [[CrossRef](#)]
- Luyben, W.L. Heat-Exchanger Bypass Control. *Ind. Eng. Chem. Res.* **2011**, *50*, 965–973. [[CrossRef](#)]
- Cheng, M.; Li, Y.; Li, Z.S.; Cai, N.S. An integrated fuel reactor coupled with an annular carbon stripper for coal-fired chemical looping combustion. *Powder Technol.* **2017**, *320*, 519–529. [[CrossRef](#)]
- Li, X.Y.; Tian, H.; Shu, G.Q.; Hu, C.; Sun, R.; Li, L.G. Effects of external perturbations on dynamic performance of carbon dioxide transcritical power cycles for truck engine waste heat recovery. *Energy* **2018**, *163*, 920–931. [[CrossRef](#)]
- Isaza, P.A.; O'Brien, A.; Warnica, W.D.; Bussmann, M. Assessing axial heat conduction in moving bed heat exchangers. *Int. J. Therm. Sci.* **2017**, *320*, 303–313. [[CrossRef](#)]
- Abdulateef, A.M.; Mat, S.; Sopian, K.; Abdulateef, J.; Gitan, A.A. Experimental and computational study of melting phase-change material in a triplex tube heat exchanger with longitudinal/triangular fins. *Sol. Energy* **2017**, *320*, 519–529. [[CrossRef](#)]
- Zi, Z.W. *Petrochemical Design Manual*; Chemical Industry Press: Beijing, China, 2015. (In Chinese)
- Wu, R.L.; Grace, J.R.; Lim, C.J. A model for heat transfer in circulating fluidized beds. *Chem. Eng. Sci.* **1990**, *45*, 3389–3398. [[CrossRef](#)]

23. Bai, Y.; Wang, X.; Si, H. Steady-state simulation of internal heat-transfer characteristics in a double tube reactor. *Chem. Eng. Process. Process Intensif.* **2019**, *144*, 107642. [[CrossRef](#)]
24. Wang, X.; Si, H. Novel concept of fluidized bed reactor design for highly efficient internal heat transfer. *Ind. Eng. Chem. Res.* **2016**, *55*, 9276–9283. [[CrossRef](#)]
25. Bai, Y.; Liu, D.C.; Si, H. A three-stage heating system of dual-fuel controlled by negative feedback for fluidized bed fast pyrolysis. *Sustain. Energy Technol. Assess.* **2021**, *46*, 101228. [[CrossRef](#)]